(Carl Zeiss Microimaging, Jena, Germany). Experiments were performed in at least five times.

### FAK Inhibitor Treatment During IVM

To inhibit the phosphorylation of FAK at Tyr397, the specific phosphorylation inhibitor FAK inhibitor 14 (Santa Cruz Biotechnology) (Golubovskaya et al., 2008) was added to the IVM medium. We prepared a 50 mM stock solution with sterile distilled water, and diluted it as necessary to a final concentration of 0, 2.5, 5.0, 10, and 25 μM. COCs were cultured for 18 hr to obtain MII oocytes.

### Quantification of Cumulus Expansion

Digital images were obtained from COCs and spatial measurements were recorded with Motic Images Plus 2.0S (Shimadzu, Kyoto, Japan). Relative cumulus expansion, defined as the ratio of the greatest distance across the COC expanded matrix (Sutton-McDowall et al., 2004; Yamashita et al., 2011) to the diameter of the oocytes inside them, was calculated for each COC after 18 hr of IVM. Experiments were performed in triplicate.

### Reverse-transcriptase Polymerase Chain Reaction

Total RNA extraction and cDNA synthesis were performed as described previously (Sakai et al., 2011), with slight modification. Total RNA was extracted from cumulus cells isolated from 20 COCs after 6 hr of IVM, and cDNA was synthesized using Cells-to-cDNA™ II (Ambion, Austin, TX). PCR was performed using Ex Taq polymerase (TaKaRa Bio, Shiga, Japan) with the following primer pairs: *Has2* sense, 5′-AAGACCC-TATGGTTGGAGGTGTT, and antisense, 5′-CATTCC-CAGAGGACCGCTTAT (167 bp); glyceraldehyde-3-phosphate dehydrogenase (*Gapdh*) (internal standard) sense, 5′-ACCACAGTCCATGCCATCAC, and antisense, 5′-TCCACCACCCTGTTGCTGTA (452 bp). Amplification conditions were as follows: 94 °C for 10 min, followed by 35 cycles of denaturation at 94 °C for 30 sec, annealing at 57 °C (*Has2*) or 58 °C (*Gapdh*) for 30 sec, and extension at 72 °C for 30 sec with a final extension at 72 °C for 5 min. PCR products were electrophoresed on 2% (w/v) agarose gels (Nippon Gene, Tokyo, Japan) and visualized with ethidium bromide (Wako) staining. The density of the band for *Has2* was normalized to the band for *Gapdh*, and the results were statistically analyzed. Experiments were performed in triplicate.

### In Vitro Fertilization and In Vitro Culture

In vitro fertilization and embryo culture were performed as described previously (Sakurai et al., 2014). The rates of fertilization (sperm penetration and the formation of two pronuclei) 4 hr after insemination in human tubal fluid (HTF) medium and blastocyst formation 120 hr after embryo culture in potassium simplex optimized medium (KSOM) were analyzed. Experiments were replicated four times.

### Blastocyst Cell Counting

Presumptive blastocysts with cavities were fixed for 10 min at room temperature and stained with Hoechst 33342 (5 μg/ml; Sigma) for 10 min at room temperature. Total cell numbers were counted using a LSM700 confocal microscope, and embryos with more than 20 cells were defined as blastocysts.

### Statistical Analysis

Significant differences in western blots were calculated using the Student's *t*-test. Statistical differences in maturation, fertilization, and blastocyst formation; relative cumulus expansion; and reverse-transcriptase PCR analysis were determined using one-way ANOVA, followed by Fisher's protected least significant differences (PLSD) test. Statistical significance was evaluated using STATVIEW (Abacus Concepts, Inc., Berkeley, CA).

## ACKNOWLEDGMENTS

This work was supported by a grant from the Japan Society for the Promotion of Science to E.S. (No. 24248047). This work was also supported in part by a Grant-in-Aid for Young Scientists (B) from the Ministry of Education, Science, and Culture, Japan to Y.H. (No. 21780250) and by JSPS KAKENHI to Y.H. (No. 26712022).

## REFERENCES

Barboni B, Mattioli M, Gioia L, Turriani M, Capacchietti G, Berardinelli P, Bernabo N. 2002. Preovulatory rise of NGF in ovine follicular fluid: Possible involvement in the control of oocyte maturation. Microsc Res Tech 59:516–521.

Biggers JD, Whittingham DG, Donahue RP. 1967. The pattern of energy metabolism in the mouse oocyte and zygote. Proc Natl Acad Sci USA 58:560–567.

Boland NI, Gosden RG. 1994. Effects of epidermal growth factor on the growth and differentiation of cultured mouse ovarian follicles. J Reprod Fertil 101:369–374.

Calalb MB, Polte TR, Hanks SK. 1995. Tyrosine phosphorylation of focal adhesion kinase at sites in the catalytic domain regulates kinase activity: A role for Src family kinases. Mol Cell Biol 15:954–963.

Calalb MB, Zhang X, Polte TR, Hanks SK. 1996. Focal adhesion kinase tyrosine-861 is a major site of phosphorylation by Src. Biochem Biophys Res Commun 228:662–668.

Carpenter G, Cohen S. 1990. Epidermal growth factor. J Biol Chem 265:7709–7712.

Chan PC, Lai JF, Cheng CH, Tang MJ, Chiu CC, Chen HC. 1999. Suppression of ultraviolet irradiation-induced apoptosis by overexpression of focal adhesion kinase in Madin–Darby canine kidney cells. J Biol Chem 274:26901–26906.

Chen HC, Appeddu PA, Isoda H, Guan JL. 1996. Phosphorylation of tyrosine 397 in focal adhesion kinase is required for binding phosphatidylinositol 3-kinase. J Biol Chem 271:26329–26334.

Chen L, Russell PT, Larsen WJ. 1993. Functional significance of cumulus expansion in the mouse: Roles for the preovulatory synthesis of hyaluronic acid within the cumulus mass. Mol Reprod Dev 34:87–93.

Cobb BS, Schaller MD, Leu TH, Parsons JT. 1994. Stable association of pp60src and pp59fyn with the focal adhesion-associated protein tyrosine kinase, pp125FAK. Mol Cell Biol 14:147–155.

Dekel N, Hillensjo T, Kraicer PF. 1979. Maturational effects of gonadotropins on the cumulus-oocyte complex of the rat. Biol Reprod 20:191–197.

Downs SM. 1989. Specificity of epidermal growth factor action on maturation of the murine oocyte and cumulus oophorus in vitro. Biol Reprod 41:371–379.

Enari M, Sakahira H, Yokoyama H, Okawa K, Iwamatsu A, Nagata S. 1998. A caspase-activated DNase that degrades DNA during apoptosis, and its inhibitor ICAD. Nature 391:43–50.

Eppig JJ. 1979. FSH stimulates hyaluronic acid synthesis by oocyte-cumulus cell complexes from mouse preovulatory follicles. Nature 281:483–484.

Eppig JJ. 1991. Intercommunication between mammalian oocytes and companion somatic cells. Bioessays 13:569–574.

Eppig JJ. 2001. Oocyte control of ovarian follicular development and function in mammals. Reproduction 122:829–838.

Fulop C, Salustri A, Hascall VC. 1997. Coding sequence of a hyaluronan synthase homologue expressed during expansion of the mouse cumulus-oocyte complex. Arch Biochem Biophys 337:261–266.

Gardner DK, Pawelczynski M, Trounson AO. 1996. Nutrient uptake and utilization can be used to select viable day 7 bovine blastocysts after cryopreservation. Mol Reprod Dev 44:472–475.

Girault JA, Costa A, Derkinderen P, Studler JM, Toutant M. 1999. FAK and PYK2/CAKbeta in the nervous system: A link between neuronal activity, plasticity and survival. Trends Neurosci 22:257–263.

Goel HL, Dey CS. 2002. Focal adhesion kinase tyrosine phosphorylation is associated with myogenesis and modulated by insulin. Cell Prolif 35:131–142.

Golubovskaya VM, Nyberg C, Zheng M, Kweh F, Magis A, Ostrov D, Cance WG. 2008. A small molecule inhibitor, 1,2,4,5-benzenetetraamine tetrahydrochloride, targeting the y397 site of focal adhesion kinase decreases tumor growth. J Med Chem 51:7405–7416.

Hanks SK, Polte TR. 1997. Signaling through focal adhesion kinase. Bioessays 19:137–145.

Harnois C, Demers MJ, Bouchard V, Vallee K, Gagne D, Fujita N, Tsuruo T, Vezina A, Beaulieu JF, Cote A, Vachon PH. 2004. Human intestinal epithelial crypt cell survival and death: Complex modulations of Bcl-2 homologs by Fak, PI3-K/Akt-1, MEK/Erk, and p38 signaling pathways. J Cell Physiol 198:209–222.

Hess KA, Chen L, Larsen WJ. 1999. Inter-alpha-inhibitor binding to hyaluronan in the cumulus extracellular matrix is required for optimal ovulation and development of mouse oocytes. Biol Reprod 61:436–443.

Hsieh M, Lee D, Panigone S, Horner K, Chen R, Theologis A, Lee DC, Threadgill DW, Conti M. 2007. Luteinizing hormone-dependent activation of the epidermal growth factor network is essential for ovulation. Mol Cell Biol 27:1914–1924.

Igishi T, Fukuhara S, Patel V, Katz BZ, Yamada KM, Gutkind JS. 1999. Divergent signaling pathways link focal adhesion kinase to mitogen-activated protein kinase cascades. Evidence for a role of paxillin in c-Jun NH(2)-terminal kinase activation. J Biol Chem 274:30738–30746.

Jin X, Han CS, Yu FQ, Wei P, Hu ZY, Liu YX. 2005. Anti-apoptotic action of stem cell factor on oocytes in primordial follicles and its signal transduction. Mol. Reprod Dev 70:82–90.

Judson PL, He X, Cance WG, Van Le L. 1999. Overexpression of focal adhesion kinase, a protein tyrosine kinase, in ovarian carcinoma. Cancer 86:1551–1556.

Khamsi F, Armstrong DT. 1997. Interactions between follicle-stimulating hormone and growth factors in regulation of deoxyribonucleic acid synthesis in bovine granulosa cells. Biol Reprod 57:684–688.

Kidder GM, Mhawi AA. 2002. Gap junctions and ovarian folliculogenesis. Reproduction 123:613–620.

Kogasaka Y, Hoshino Y, Hiradate Y, Tanemura K, Sato E. 2013. Distribution and association of mTOR with its cofactors, raptor and rictor, in cumulus cells and oocytes during meiotic maturation in mice. Mol Reprod Dev 80:334–348.

Longo FJ, Chen DY. 1985. Development of cortical polarity in mouse eggs: Involvement of the meiotic apparatus. Dev Biol 107:382–394.

Lorenzo PL, Illera MJ, Illera JC, Illera M. 1994. Enhancement of cumulus expansion and nuclear maturation during bovine oocyte maturation in vitro by the addition of epidermal growth factor and insulin-like growth factor I. J Reprod Fertil 101:697–701.

Lorenzo PL, Rebollar PG, Illera MJ, Illera JC, Illera M, Alvarino JM. 1996. Stimulatory effect of insulin-like growth factor I and epidermal growth factor on the maturation of rabbit oocytes in vitro. J Reprod Fertil 107:109–117.

Lunn JA, Jacamo R, Rozengurt E. 2007. Preferential phosphorylation of focal adhesion kinase tyrosine 861 is critical for mediating an anti-apoptotic response to hyperosmotic stress. J Biol Chem 282:10370–10379.

Luo J, McGinnis LK, Kinsey WH. 2009. Fyn kinase activity is required for normal organization and functional polarity of the mouse oocyte cortex. Mol Reprod Dev 76:819–831.

McGinnis LK, Albertini DF, Kinsey WH. 2007. Localized activation of Src-family protein kinases in the mouse egg. Dev Biol 306:241–254.

McGinnis LK, Luo J, Kinsey WH. 2013. Protein tyrosine kinase signaling in the mouse oocyte cortex during sperm-egg interactions and anaphase resumption. Mol Reprod Dev 80: 260–272.

Meng XQ, Zheng KG, Yang Y, Jiang MX, Zhang YL, Sun QY, Li YL. 2006. Proline-rich tyrosine kinase2 is involved in F-actin organization during in vitro maturation of rat oocyte. Reproduction 132:859–867.

Mitra SK, Hanson DA, Schlaepfer DD. 2005. Focal adhesion kinase: In command and control of cell motility. Nat Rev Mol Cell Biol 6:56–68.

Mizutani T, Shiraishi K, Welsh T, Ascoli M. 2006. Activation of the lutropin/choriogonadotropin receptor in MA-10 cells leads to the tyrosine phosphorylation of the focal adhesion kinase by a pathway that involves Src family kinases. Mol Endocrinol 20:619–630.

Nagano M, Hoshino D, Koshikawa N, Akizawa T, Seiki M. 2012. Turnover of focal adhesions and cancer cell migration. Int J Cell Biol 2012:310616.

Noma N, Kawashima I, Fan HY, Fujita Y, Kawai T, Tomoda Y, Mihara T, Richards JS, Shimada M. 2011. LH-induced neuregulin 1 (NRG1) type III transcripts control granulosa cell differentiation and oocyte maturation. Mol Endocrinol 25:104–116.

Okamura Y, Myoumoto A, Manabe N, Tanaka N, Okamura H, Fukumoto M. 2001. Protein tyrosine kinase expression in the porcine ovary. Mol Hum Reprod 7:723–729.

Owen JD, Ruest PJ, Fry DW, Hanks SK. 1999. Induced focal adhesion kinase (FAK) expression in FAK-null cells enhances cell spreading and migration requiring both auto- and activation loop phosphorylation sites and inhibits adhesion-dependent tyrosine phosphorylation of Pyk2. Mol Cell Biol 19:4806–4818.

Owen KA, Pixley FJ, Thomas KS, Vicente-Manzanares M, Ray BJ, Horwitz AF, Parsons JT, Beggs HE, Stanley ER, Bouton AH. 2007. Regulation of lamellipodial persistence, adhesion turnover, and motility in macrophages by focal adhesion kinase. J Cell Biol 179:1275–1287.

Park JY, Su YQ, Ariga M, Law E, Jin SL, Conti M. 2004. EGF-like growth factors as mediators of LH action in the ovulatory follicle. Science 303:682–684.

Pelech S, Jelinkova L, Susor A, Zhang H, Shi X, Pavlok A, Kubelka M, Kovarova H. 2008. Antibody microarray analyses of signal transduction protein expression and phosphorylation during porcine oocyte maturation. J Proteome Res 7:2860–2871.

Preis KA, Seidel G, Jr., Gardner DK. 2005. Metabolic markers of developmental competence for in vitro-matured mouse oocytes. Reproduction 130:475–483.

Richards JS, Russell DL, Ochsner S, Hsieh M, Doyle KH, Falender AE, Lo YK, Sharma SC. 2002. Novel signaling pathways that control ovarian follicular development, ovulation, and luteinization. Recent Prog Horm Res 57:195–220.

Russell DL, Robker RL. 2007. Molecular mechanisms of ovulation: Co-ordination through the cumulus complex. Hum Reprod Update 13:289–312.

Sakai C, Hoshino Y, Sato Y, Sato E. 2011. Evaluation of maturation competence of metaphase II oocytes in mice based on the distance between pericentriolar materials of meiotic spindle: distance of PCM during oocyte maturation. J Assist Reprod Genet 28:157–166.

Sakurai M, Ohtake J, Ishikawa T, Tanemura K, Hoshino Y, Arima T, Sato E. 2012. Distribution and Y397 phosphorylation of focal adhesion kinase on follicular development in the mouse ovary. Cell Tissue Res 347:457–465.

Sakurai M, Sato Y, Mukai K, Suematsu M, Fukui E, Yoshizawa M, Tanemura K, Hoshino Y, Matsumoto H, Sato E. 2014. Distribution of tubulointerstitial nephritis antigen-like 1 and structural matrix proteins in mouse embryos during preimplantation development in vivo and in vitro. Zygote 22:259–265.

Salustri A, Yanagishita M, Underhill CB, Laurent TC, Hascall VC. 1992. Localization and synthesis of hyaluronic acid in the cumulus cells and mural granulosa cells of the preovulatory follicle. Devel Biol 151:541–551.

Sanders MA, Basson MD. 2000. Collagen IV-dependent ERK activation in human Caco-2 intestinal epithelial cells requires focal adhesion kinase. Journal Biol Chem 275:38040–38047.

Schaller MD, Borgman CA, Cobb BS, Vines RR, Reynolds AB, Parsons JT. 1992. pp125FAK a structurally distinctive protein-tyrosine kinase associated with focal adhesions. Proc Natl Acad Sci USA 89:5192–5196.

Schaller MD, Hildebrand JD, Shannon JD, Fox JW, Vines RR, Parsons JT. 1994. Autophosphorylation of the focal adhesion kinase, pp125FAK, directs SH2-dependent binding of pp60src. Mol Cell Biol 14:1680–1688.

Schlaepfer DD, Hanks SK, Hunter T, van der Geer P. 1994. Integrin-mediated signal transduction linked to Ras pathway by GRB2 binding to focal adhesion kinase. Nature 372:786–791.

Schlaepfer DD, Hunter T. 1996. Evidence for in vivo phosphorylation of the Grb2 SH2-domain binding site on focal adhesion kinase by Src-family protein-tyrosine kinases. Mol Cell Biol 16:5623–5633.

Schlaepfer DD, Hunter T. 1997. Focal adhesion kinase overexpression enhances ras-dependent integrin signaling to ERK2/mitogen-activated protein kinase through interactions with and activation of c-Src. J Biol Chem 272:13189–13195.

Schwartz MA, Schaller MD, Ginsberg MH. 1995. Integrins: Emerging paradigms of signal transduction. Annu Rev Cell Dev Biol 11:549–599.

Serrels B, Serrels A, Brunton VG, Holt M, McLean GW, Gray CH, Jones GE, Frame MC. 2007. Focal adhesion kinase controls

actin assembly via a FERM-mediated interaction with the Arp2/3 complex. Nat Cell Biol 9:1046–1056.

Sharma D, Kinsey WH. 2013. PYK2: A calcium-sensitive protein tyrosine kinase activated in response to fertilization of the zebrafish oocyte. Dev Biol 373:130–140.

Shimada M, Hernandez-Gonzalez I, Gonzalez-Robayna I, Richards JS. 2006. Paracrine and autocrine regulation of epidermal growth factor-like factors in cumulus oocyte complexes and granulosa cells: Key roles for prostaglandin synthase 2 and progesterone receptor. Mol Endocrinol 20:1352–1365.

Singh B, Barbe GJ, Armstrong DT. 1993. Factors influencing resumption of meiotic maturation and cumulus expansion of porcine oocyte–cumulus cell complexes in vitro. Mol Reprod Dev 36:113–119.

Sirotkin AV, Dukesova J, Pivko J, Makarevich AV, Kubek A. 2002. Effect of growth factors on proliferation, apoptosis and protein kinase A expression in cultured porcine cumulus oophorus cells. Reprod Nutr Dev 42:35–43.

Sonoda Y, Matsumoto Y, Funakoshi M, Yamamoto D, Hanks SK, Kasahara T. 2000. Anti-apoptotic role of focal adhesion kinase (FAK). Induction of inhibitor-of-apoptosis proteins and apoptosis suppression by the overexpression of FAK in a human leukemic cell line, HL-60. J Biol Chem 275:16309–16315.

Sood AK, Coffin JE, Schneider GB, Fletcher MS, DeYoung BR, Gruman LM, Gershenson DM, Schaller MD, Hendrix MJ. 2004. Biological significance of focal adhesion kinase in ovarian cancer: Role in migration and invasion. Am J Pathol 165:1087–1095.

Susin SA, Daugas E, Ravagnan L, Samejima K, Zamzami N, Loeffler M, Costantini P, Ferri KF, Irinopoulou T, Prevost MC, Brothers G, Mak TW, Penninger J, Earnshaw WC, Kroemer G. 2000. Two distinct pathways leading to nuclear apoptosis. J Exp Med 192:571–580.

Sutton-McDowall ML, Gilchrist RB, Thompson JG. 2004. Cumulus expansion and glucose utilisation by bovine cumulus-oocyte complexes during in vitro maturation: The influence of glucosamine and follicle-stimulating hormone. Reproduction 128:313–319.

Svitkina TM, Borisy GG. 1999. Arp2/3 complex and actin depolymerizing factor/cofilin in dendritic organization and treadmilling of actin filament array in lamellipodia. J Cell Biol 145: 1009–1026.

Thomas SM, Brugge JS. 1997. Cellular functions regulated by Src family kinases. Annu Rev Cell Dev Biol 13:513–609.

Vanderhyden B. 2002. Molecular basis of ovarian development and function. Front Biosci 7:d2006–2022.

Vivanco I, Sawyers CL. 2002. The phosphatidylinositol 3-Kinase AKT pathway in human cancer. Nat Rev Cancer 2:489–501.

Wang HB, Dembo M, Hanks SK, Wang Y. 2001. Focal adhesion kinase is involved in mechanosensing during fibroblast migration. Proc Natl Acad Sci U S A 98:11295–11300.

Yamashita Y, Kawashima I, Yanai Y, Nishibori M, Richards JS, Shimada M. 2007. Hormone-induced expression of tumor necrosis factor alpha-converting enzyme/A disintegrin and metalloprotease-17 impacts porcine cumulus cell oocyte complex expansion and meiotic maturation via ligand activation of the epidermal growth factor receptor. Endocrinology 148:6164–6175.

Yamashita Y, Okamoto M, Kawashima I, Okazaki T, Nishimura R, Gunji Y, Hishinuma M, Shimada M. 2011. Positive feedback loop between prostaglandin E2 and EGF-like factors is essential for sustainable activation of MAPK3/1 in cumulus cells during in vitro maturation of porcine cumulus oocyte complexes. Biol Reprod 85:1073–1082.

Zachary I, Rozengurt E. 1992. Focal adhesion kinase (p125FAK): A point of convergence in the action of neuropeptides, integrins, and oncogenes. Cell 71:891–894.

Zheng KG, Meng XQ, Yang Y, Yu YS, Liu DC, Li YL. 2007. Requirements of Src family kinase during meiotic maturation in mouse oocyte. Mol Reprod Dev 74:125–130.

Zheng Y, Yang W, Xia Y, Hawke D, Liu DX, Lu Z. 2011. Ras-induced and extracellular signal-regulated kinase 1 and 2 phosphorylation-dependent isomerization of protein tyrosine phosphatase (PTP)-PEST by PIN1 promotes FAK dephosphorylation by PTP-PEST. Mol Cell Biol 31:4258–4269.

## SUPPORTING INFORMATION

Additional supporting information may be found in the online version of this article at the publisher's web-site.

frontiers in Neuroscience

ORIGINAL RESEARCH
published: 31 March 2016
doi: 10.3389/fnins.2016.00137

# Prenatal Exposure to Arsenic Impairs Behavioral Flexibility and Cortical Structure in Mice

*Kyaw H. Aung[1,2], Chaw Kyi-Tha-Thu[1], Kazuhiro Sano[3], Kazuaki Nakamura[2], Akito Tanoue[2], Keiko Nohara[3], Masaki Kakeyama[4], Chiharu Tohyama[5], Shinji Tsukahara[1] and Fumihiko Maekawa[3]**

[1] Division of Life Science, Saitama University, Saitama, Japan, [2] Department of Pharmacology, National Research Institute for Child Health and Development, Setagaya, Japan, [3] Molecular Toxicology Section, National Institute for Environmental Studies, Tsukuba, Japan, [4] Faculty of Human Sciences, Waseda University, Tokorozawa, Japan, [5] Faculty of Medicine, University of Tsukuba, Tsukuba, Japan

Exposure to arsenic from well water in developing countries is suspected to cause developmental neurotoxicity. Although, it has been demonstrated that exposure to sodium arsenite ($NaAsO_2$) suppresses neurite outgrowth of cortical neurons *in vitro*, it is largely unknown how developmental exposure to $NaAsO_2$ impairs higher brain function and affects cortical histology. Here, we investigated the effect of prenatal $NaAsO_2$ exposure on the behavior of mice in adulthood, and evaluated histological changes in the prelimbic cortex (PrL), which is a part of the medial prefrontal cortex that is critically involved in cognition. Drinking water with or without $NaAsO_2$ (85 ppm) was provided to pregnant C3H mice from gestational days 8 to 18, and offspring of both sexes were subjected to cognitive behavioral analyses at 60 weeks of age. The brains of female offspring were subsequently harvested and used for morphometrical analyses. We found that both male and female mice prenatally exposed to $NaAsO_2$ displayed an impaired adaptation to repetitive reversal tasks. In morphometrical analyses of Nissl- or Golgi-stained tissue sections, we found that $NaAsO_2$ exposure was associated with a significant increase in the number of pyramidal neurons in layers V and VI of the PrL, but not other layers of the PrL. More strikingly, prenatal $NaAsO_2$ exposure was associated with a significant decrease in neurite length but not dendrite spine density in all layers of the PrL. Taken together, our results indicate that prenatal exposure to $NaAsO_2$ leads to behavioral inflexibility in adulthood and cortical disarrangement in the PrL might contribute to this behavioral impairment.

**Keywords: sodium arsenite, developmental neurotoxicity, behavioral impairment, neurite outgrowth, prelimbic cortex**

OPEN ACCESS

***Edited by:***
*Riccarda Granata, University of Turin, Italy*

***Reviewed by:***
*Maria E. Gonsebatt, Universidad Nacional Autónoma de México, Mexico*
*Andrea Allan, University of New Mexico, USA*

****Correspondence:***
*Fumihiko Maekawa*
*fmaekawa@nies.go.jp*

***Specialty section:***
*This article was submitted to Neuroendocrine Science, a section of the journal Frontiers in Neuroscience*

***Received:*** *21 December 2015*
***Accepted:*** *17 March 2016*
***Published:*** *31 March 2016*

***Citation:***
*Aung KH, Kyi-Tha-Thu C, Sano K, Nakamura K, Tanoue A, Nohara K, Kakeyama M, Tohyama C, Tsukahara S and Maekawa F (2016) Prenatal Exposure to Arsenic Impairs Behavioral Flexibility and Cortical Structure in Mice. Front. Neurosci. 10:137. doi: 10.3389/fnins.2016.00137*

## INTRODUCTION

The developing brain is vulnerable to disruption by environmental factors including toxic chemical exposure. Environmental exposures may therefore account for an increase in the prevalence of neurodevelopmental and neuropsychiatric disorders including autism spectrum disorders, attention deficit hyperactivity disorders (ADHD), and learning disabilities (Grandjean and Landrigan, 2006, 2014). Recent studies suggest that *in utero* and lactational exposure to

toxic chemicals affects the development of the brain. For example, exposure to inorganic lead, methylmercury, and polychlorinated biphenyls during gestation and early childhood are associated with the prevalence of mental retardation, cerebral palsy, and ADHD in children (Grandjean and Landrigan, 2006; Bisen-Hersh et al., 2014). These studies indicate that early life environmental exposures play a role in the etiology of neurodevelopmental disorders.

It has been long suspected that arsenic exposure can lead to developmental neurotoxicity. More than 200 million people worldwide have been estimated to be chronically exposed to arsenic in drinking water at concentrations above the World Health Organization (WHO) recommended safety limit of 10 μg/L (WHO, 2008). A large number of epidemiological studies have demonstrated that chronic exposure to arsenic produces peripheral neuropathies and decreases cognitive performance in children such as lowered memory and intelligence quotient scores on standardized tests (Rocha-Amador et al., 2007; Rosado et al., 2007; Wasserman et al., 2007), which are indicative of higher brain function deficits. Additionally, follow-up studies on victims of arsenic poisoning from the Morinaga formula incident in Japan revealed an association between oral exposure to arsenic during infancy and various brain disorders, including mental retardation and epilepsy (Dakeishi et al., 2006). These studies suggest that early life arsenic exposure can affect higher brain function later in life. This notion is supported by some studies in animal models. For example, exposure to low level arsenic in maternal drinking water throughout gestational and lactational period increased indices of anxiety in mouse offspring during a novel object exploration task (Martinez-Finley et al., 2009). Moreover, few behavioral deficits such as an increase in pivoting, a type of abnormal gait behavior, was observed in younger mouse offspring following a short period of gestational exposure to arsenic (Colomina et al., 1996).

Arsenic exposure could produce behavioral changes through effects on the developing brain directly since arsenic freely crosses the fetus-placenta and blood-brain barrier in human (Willhite and Ferm, 1984; Hirner and Rettenmeier, 2010). *In vitro* and *in vivo* experimental models have been used to elucidate how arsenic exposure impairs higher brain function. A previous study showed that sodium arsenite ($NaAsO_2$) exposure produces both apoptotic and necrotic cell death in developing brain cells in rat (Chattopadhyay et al., 2002). Our *in vitro* studies have shown that $NaAsO_2$ exposure induces apoptotic cell death and inhibits neuritogenesis (Koike-Kuroda et al., 2010; Aung et al., 2013). The inhibitory effect of $NaAsO_2$ on neuritogenesis is in part result from alterations in cytoskeletal components (Aung et al., 2013) and the downregulation of AMPA receptors, which are known to regulate the expression of cytoskeletal proteins (Maekawa et al., 2013). In animal studies, embryonic arsenic exposure produces neural tube defects, increase neuronal apoptosis, disrupt neural outgrowth, and reduce overall head size in both mouse and zebrafish models (Chaineau et al., 1990; Li et al., 2009). Further, it has been reported that arsenic exposure in rats from gestation throughout lactation and development until the age of 4 month alters morphology of nerve fibers and axon in the corpus striatum (Rios et al., 2009). These studies indicate that structural changes of brain such as neural network formation might contribute to the impairment of higher brain function following early life exposure to $NaAsO_2$. However, the precise mechanism by which developmental arsenic exposure produces impairments in higher brain function remains largely unknown.

Executive function such as planning, goal-directed action, and behavioral flexibility are core units of higher brain function, and impairment of these functions has been observed in a variety of neurodevelopmental disorders (Valencia et al., 1992; Kipp, 2005; Hill and Bird, 2006). To evaluate these executive processes in mice, a model of behavioral flexibility was recently established using the IntelliCage system, which is a fully automated behavioral testing apparatus for mice under group-housing conditions (Endo et al., 2011, 2012). This testing apparatus allows for the comprehensive and reproducible evaluation of behavioral flexibility. In humans, the brain areas responsible for executive function of goal-directed actions and behavioral flexibility are located in the medial prefrontal cortex (Yan et al., 2015). Several studies have shown that the prelimbic cortex (PrL), a part of the medial prefrontal cortex, is critically involved in a variety of cognitive and executive processes (Dalley et al., 2004; Marquis et al., 2007; Ragozzino, 2007). It has been also reported that the PrL is affected by exposure to chemicals, such as methylmercury, lead, and dioxin, and that exposure-associated impairments in the PrL are associated with decreased executive function in rodents (Ferraro et al., 2009; Tomasini et al., 2012). Accordingly, we decided to investigate the structure of the PrL as a possible target of arsenic-induced brain impairment.

In the present study, we used a fully automated behavioral analysis system to investigate the effects of prenatal $NaAsO_2$ exposure on murine behavioral flexibility in adulthood, and then analyzed the morphology of neuronal cells in these animals in order to determine how early life $NaAsO_2$ exposure produces neurotoxicity.

## MATERIALS AND METHODS

### Animals and $NaAsO_2$ Exposure

Pregnant C3H mice were purchased from JAPAN SLC (Shizuoka, Japan) and housed on a 12-h light/dark cycle at a temperature of 24 ± 1°C with free access to water and food. From gestational days 8–18, pregnant females were given *ad libitum* access to regular water or water containing 85 parts per million (ppm) $NaAsO_2$ (equivalent to 85 mg/L). To examine the water consumption of pregnant dams, the weight of water bottle for each dam was measured before and after providing *ad libitum* access to water. Pregnant dams tolerated the dose of $NaAsO_2$ at 85 ppm, and no obvious effects on maternal toxicity or teratogenicity were observed.

The pups were weaned at post-natal day 21 and housed under the same conditions as the dams. The number and sex of pups born from dams were then measured. At 60 weeks of age, control and $NaAsO_2$-exposed offspring were prepared for behavioral flexibility testing using the IntelliCage system (TSE Systems GmbH, Bad Homburg, Germany). Mice were randomly selected per dams (number of dams: control = 6 and $NaAsO_2$ = 9) to minimize the litter effects. After selecting mice, they were lightly

anesthetized with diethyl ether and subcutaneously implanted with a glass-covered transponder. Each transponder had a unique ID code for radiation frequency identification (RFID) for use with the IntelliCage system. Males and females were separately tested using different IntelliCage apparatuses. The control and $NaAsO_2$-exposed groups includes 9 mice per group for females and 6 or 10 mice per group for males. All procedures were approved by the Institutional Animal Care and Use Committee of the National Institute for Environmental Studies (NIES) and conducted strictly in accordance with NIES guidelines.

## Intellicage Apparatus

The IntelliCage is a computer-based, fully-automated testing apparatus that can be used to monitor the spontaneous and cognitive behaviors of group-housed RFID-tagged mice in a large home cage (**Figure 1A**). Briefly, a large standard plastic cage (55 × 37.5 × 20.5 $cm^3$) was equipped with four triangular operant learning chambers (hereafter referred to as corners) (15 × 15 × 21 $cm^3$) that fit into each corner of the cage. RFID readers and other sensors allowed the simultaneous monitoring of up to 16 transponder-tagged mice living in the same cage. Mice were allowed to enter each corner (hereafter referred to as a "corner visit") through a short, narrow tunnel that functioned as an RFID antenna. Only one mouse was able to enter a given corner at any one time due to the limited size of the tunnel. In the inner space of each corner was equipped with two nose poke holes that were monitored via an infrared beam-break response detector. Nose poke behavior triggered to open a motorized gate access to a water bottle nipple. For each behavioral event (corner visit, nose poke, and licking), mouse ID and corner ID were automatically recorded through the RFID readers, infrared sensors, and lickometers.

## Intellicage Test Procedures

### Acclimation

The control and $NaAsO_2$-exposed male or female mice at 67 weeks of age were separately introduced to IntelliCage apparatuses on the same day. The number of mice in each IntelliCage apparatus was counterbalanced within groups. Acclimation and behavioral tests were then conducted according to test procedures. In acclimation phase 1 (3 days), the motorized gates controlling access to water bottle nipples were kept open in all 4 corners; thus, mice were allowed to drink water in each corner *ad libitum*. In acclimation phase 2 (1 day), the mice were trained to perform the nose poke task. Initially, all motorized gates were closed and mice were only given access to water bottle nipples after a nose poke event. The gate remained open for 4 sec following each nose poke, and water was available through the nose poke task for 24 h. In acclimation phase 3 (5 days), mice were only given the opportunity to gain access to water through the nose poke task for a 3-h period (19:00–22:00) per day. During acclimation phase, four female mice (one from control group and three from $NaAsO_2$-exposed group) were not able to learn how to access water drinkable corners, and such mice were not used in the following behavioral tasks.

### Behavioral Sequencing Task

The behavioral flexibility test, also referred to as the behavioral sequencing task, was composed of an acquisition phase and a serial reversal task phase. The acquisition phase consisted of 11 or 21 sessions of the behavioral sequencing task (**Figure 1B**) and the serial reversal task phase consisted of repetitions of a reversal task (Rev. 1−11, **Figure 1C**). Water-deprived mice had 4 sec of access to water as a reward when they visited designated corners during a daily 3-h test session (19:00−22:00; **Figure 1D**). A total of 67 sessions for male mice and 83 sessions for female mice were conducted. In each session, mice were rewarded continuously if they alternated visits between two particular diagonally opposed corners (**Figure 1C**). The diagonal pair of corners was either active or inactive in a mutually exclusive manner, meaning that there was always one active reward corner, one inactive reward corner, and two never-rewarded corners. Mice were able to open the gate in an active corner by nose poke, and the gate remained open for 4 s to permit drinking. After the reward period, the corner instantly became inactive, and this signal was synchronized with the activation of the diagonally opposed corner. The alteration of corner assignments was controlled for each mouse independently by the IntelliCage software. Thus, the mice had to alternate between two diagonally opposed reward corners in order to acquire rewards continuously. A visit to either of the two never-rewarded corners was regarded as a discrimination error. The number of discrimination errors within the first 100 visits in each session provided a discrimination error rate that was used to analyze inter-session learning performance.

## Histological Staining

After the last session of behavioral experiments, the same female mice were immediately sacrificed for morphometrical analysis of neuronal cells, while male mice were used for gene expression analyses (not described in this study). Mice were deeply anesthetized with sodium pentobarbital (60 mg/kg) and brains were harvested for analysis. Brains were histologically processed using the FD Rapid GolgiStain Kit (FD NeuroTechnologies, Ellicot City, MD, USA). Briefly, brains were rinsed with distilled water, immersed in 5 mL of equal parts Solution A and Solution B at room temperature, and stored for 2 weeks in the dark. Storage solution was replaced with fresh solution on the second day. Tissues were next immersed in Solution C at 4°C for at least 48 h. Solution C was replaced with fresh solution on the second day. Samples were then quickly frozen at −70°C and stored at −20°C until use. Coronal brain sections (60 μm) were cut using a cryostat (Leica CM1900; Leica Microsystems, Wetzlar, Germany), where the temperature of chamber and specimen head were set to −22°C and −23°C, respectively. Brain sections were mounted on gelatin-coated glass slides and allowed to dry at room temperature. Sections were then stained with a solution of 1 part Solution D, 1 part Solution E, and 2 parts distilled water for 10 min at room temperature. Golgi-stained brain sections were rinsed in distilled water twice for 4 min each and counterstained with 0.1% Cresyl Fast Violet solution. The Golgi- and Cresyl Fast Violet-stained sections were used for stereological analysis. The group average number of neurons and glial cells, length of

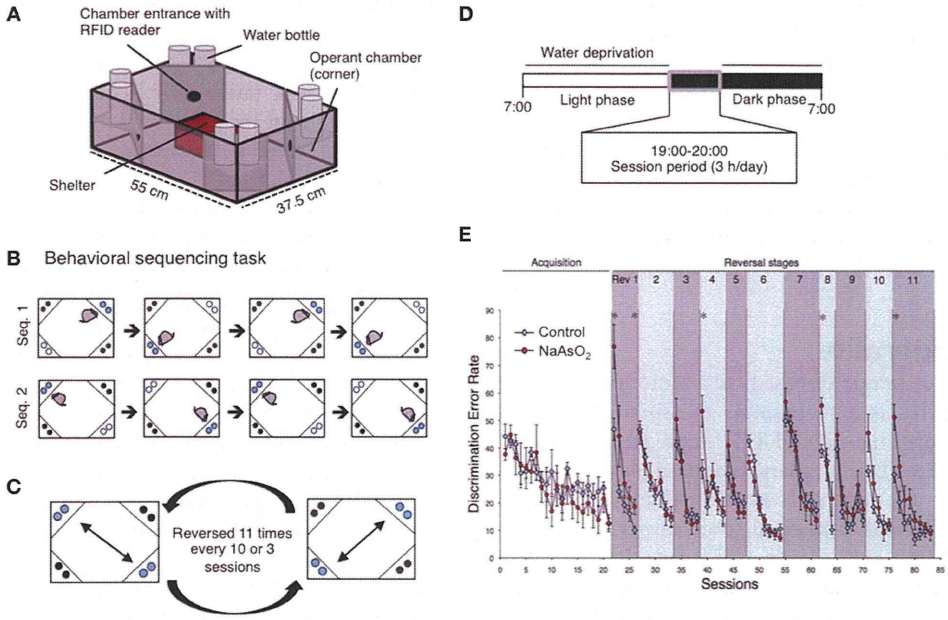


**FIGURE 1 | Impaired behavioral flexibility in adult mice born to dams that were administered $NaAsO_2$ during gestation. (A)** Overview of an IntelliCage apparatus. **(B)** Behavioral sequencing task. Mice were allowed to make an access to water as a reward for 4 s during their visits at an active reward corner (blue circle). The location of the active reward corner was automatically alternated to a diagonally opposed corner each time the mouse received a reward. Therefore, mice obtained rewards continuously by acquiring a behavioral sequence (alternating between the two reward corners). A visit to a never-rewarded corner (black circle) was counted as a discrimination error. **(C)** Serial reversal task. For each mouse, the assigned spatial patterns of the rewarded corners (sequence 1 or sequence 2) were reversed 11 times every 3 or 8 sessions. **(D)** Timeline of the experiment for each day. **(E)** Learning performance of control or $NaAsO_2$-exposed female mice in the behavioral flexibility test. Discrimination error rates (the number of discrimination errors in the first 100 corner visits of a session) are expressed as mean ± SEM (control group $n = 8$, $NaAsO_2$-exposed group $n = 6$). An asterisk indicates a statistical difference ($p < 0.05$) from the control group.

neurites, and density of dendritic spines were calculated from five or seven brains of mice, which was randomly selected and blind from behavioral data, for control and $NaAsO_2$-exposed group, respectively.

## Stereological Analysis of the Length of Neurites and the Number of Neuronal Cells

The length of neurites and the number of neurons and glial cells in the PrL were measured using StereoInvestigator software (MicroBrightField (MBF) Bioscience, Williston, VT., USA) and a light microscope (DM5000B; Leica Microsystems) connected to a CCD camera. The boundaries between the PrL and the infralimbic cortex (IL) and between the PrL and the dorsal anterior cingulate (ACd) were determined by observing differences in cell size and density in the cortical layers of Cresyl Fast Violet-stained brain sections (Van De Werd et al., 2010). The rostrocaudal level of the PrL was determined by referring to an atlas of the mouse brain (Franklin and Paxinos, 2008; **Figure 2A**).

The length of neurites on Golgi-stained neurons in the left PrL was measured using the Space Ball probe utility of the Stereo Investigator software. The contours of the PrL in each brain section were drawn using a 5X objective lens magnification according to the criteria mentioned above. We set grid sizes of 150 × 200 μm, and used a sphere with a 40-μm radius and a highest top guard zone of 2.5 μm for the quantification of neurite length. The intersectional points between Golgi-stained neurites and the spherical line (**Figure 3B**) were counted in three consecutive sections of the PrL using a 100X oil immersion objective lens magnification, and the number of intersection points was used to compute the estimated length of Golgi-stained neurite in the selected region of the PrL for each mice (Mouton et al., 2002). The estimated length of Golgi-stained neurite was then normalized by dividing it by the estimated volume of the selected region in each animal. The coefficient of error (Gundersen, $m = 1$) for the estimation of neurite length was 0.05–0.09 for each animal.

The optical fractionator method was used to measure the number of Cresyl Fast Violet-stained neurons (pyramidal and non-pyramidal neurons) and glial cells in three different cortical layers (layer II–III, V, and VI) of the left PrL in accordance with the system work flow of the Stereo Investigator software. Since cortical layer IV is completely disappeared in the mice PrL (Van De Werd et al., 2010), it was not included in this analysis. The cortical layer boundaries were distinguished based on differences in cell size and density in Cresyl Fast Violet-stained brain sections (**Figure 2B**). The contours for layers II–III, V, and VI were drawn in each section using a 5X objective lens magnification and a frame size of 30 × 30 μm within the grid size of 150 × 150 μm. The height of the optical dissector was 40 μm and the top guard zone was 2.5 μm. Cell numbers were counted manually

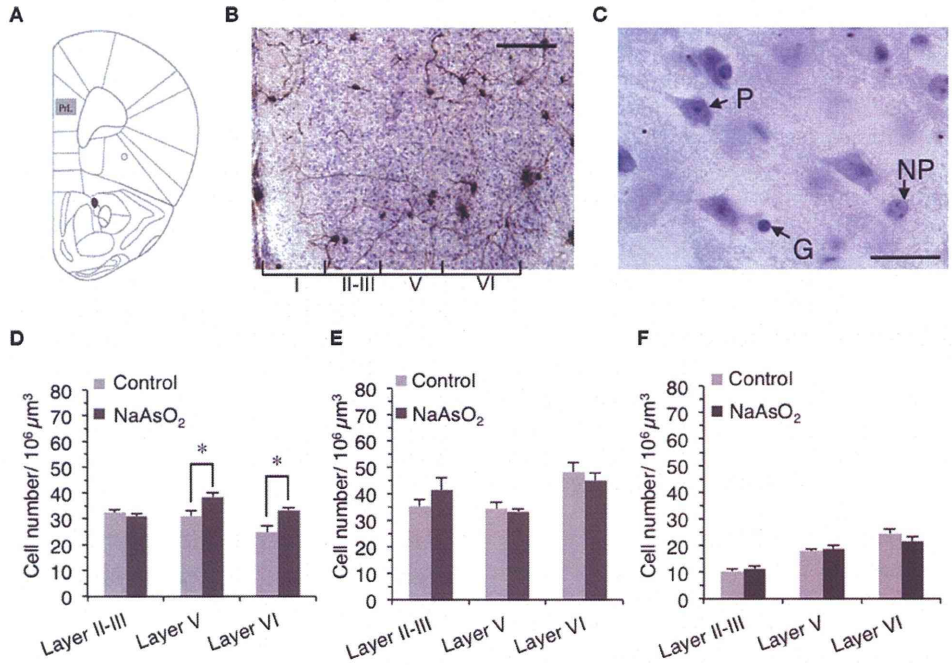


**FIGURE 2 | Alteration in the number of neuronal cells in the PrL of adult female mice born to dams that were administered $NaAsO_2$. (A)** Illustration of the region of interest, the PrL, adapted from a mouse brain atlas (Franklin and Paxinos, 2008). **(B)** Representative photomicrograph of the PrL in Golgi- and Cresyl Fast Violet-stained coronal brain sections. The Greek numbered (I–VI) regions indicate the cortical layers of the PrL. Scale bar = 20 μm. **(C)** Photomicrographs of the PrL at high magnification showing a Cresyl Fast Violet-stained pyramidal neuron (P), a non-pyramidal neuron (NP), and a glial cell (G). The length of scale bar indicates 5 μm. The number of pyramidal neurons **(D)**, non-pyramidal neurons **(E)**, and glial cells **(F)** in the PrL. Values are expressed as mean ± SEM (control group $n = 7$, $NaAsO_2$-exposed groups $n = 5$). An asterisk indicates $p < 0.05$ vs. the control group.

using a 100X oil immersion objective lens magnification. The setting for cell counting was sufficient to generate a coefficient of error (Gundersen, $m = 1$) of 0.05–0.06. The estimated number of pyramidal neurons, non-pyramidal neurons, and glial cells in each layer of the PrL was normalized by dividing each number by the estimated volume of its respective layer. The morphological criteria used to identify neuronal and glial cells observed in Cresyl Fast Violet-stained brain sections have been previously reported (Tsukahara et al., 2011). To distinguish pyramidal neurons from non-pyramidal neurons, the following criteria were used: (1) the cell bodies of pyramidal neurons exhibited a characteristic triangular shape with a single large apical dendrite extending vertically toward the pial surface, (2) non-pyramidal neurons were identified by the absence of the preceding criteria and exhibited a relatively smaller cell body size than that of pyramidal neurons (**Figure 2C**).

## Imaging and Analysis of Dendritic Spine Morphology

The dendritic segments of Golgi-stained pyramidal neurons were used in morphometrical analyses. Sequential z-series images of dendritic segments were taken every 0.4 μm with an oil immersion lens (Plan Apo VC 100X, Numerical Aperture 1.40, Oil; Nikon, Tokyo, Japan) and a BioRevo 9000 microscope (Keyence Co., Osaka, Japan). The applied zoom factor (1.5X) provided images with 0.14 μm/pixel resolution. Images were then deconvoluted using Keyence BZ II Analyzer software (Keyence) and constructed into three-dimensional images using ImageJ software (National Institutes of Health, Bethesda, MD, USA) for analyses of dendritic spine morphology. The density and head diameter of dendritic spines were analyzed using Spiso-3D automated dendritic spine analysis software, which has an equivalent capacity to Neurolucida (MBF Bioscience, USA) (Mukai et al., 2011). The primary basilar dendritic segments of Golgi-stained pyramidal neurons, lying between 10 and 100 μm from the soma, were used to analyze the morphology of dendritic spines. For each cortical layer (layer II–III, V, or VI), 30–45 dendritic segments were analyzed per experimental group. Spine density was calculated from the number of spines existing on the total length of 40–100 μm dendritic segments. To examine spine morphological changes in response to prenatal $NaAsO_2$ exposure, the diameter of the spine head was classified into three categories: (1) small-head spines with a diameter of 0.2–0.4 μm, (2) middle-head spines with a diameter of 0.4–0.5 μm, and (3) large-head spines with a diameter of 0.5–1 μm.

## Statistical Analysis

Changes in mouse behavioral flexibility were analyzed using the non-parametric Mann Whitney *U*-test with R software (The R Foundation for Statistical Computing, Vienna, Austria) because

the sample size of each group for each session was relatively small and it didn't follow a normal distribution. Morphometrical and other general assessments (including body weight, number of pups, and water intake) were analyzed with the parametric Student's unpaired *t*-test with Welch's correction with Prism software (GraphPad Software, La Jolla, CA, USA). Statistical differences were evaluated between the control and $NaAsO_2$-exposed groups. $P \leq 0.05$ were considered to be statistically significant.

# RESULTS

## Maternal and Embryonic Toxicity

No dams were found to develop significant abnormalities in general health parameters including the body weight gain of the dams during pregnancy (Figure S1) and maternal death. In addition, there were no differences in the number of live pups between the control and $NaAsO_2$-exposed groups (Figure S2).

## Basal Activity Levels of Offspring

No toxic effects of prenatal $NaAsO_2$ exposure on body weight gain and blood glucose level of offspring were observed (Figure S3). In addition, there were no apparent differences in most of basal activity indices of the offspring in the acclimation phase of the behavioral flexibility test were observed between the two groups, except significant increase in duration of nose poke in $NaAsO_2$-exposed female mice (Tables S1, S2).

## Impaired Behavioral Flexibility in $NaAsO_2$-Exposed Mice

Behavioral flexibility was examined by evaluating the number of incorrectly visiting the two never-rewarding corner within the first 100 visits of a given test session (discrimination error rate). In acquisition phase of the behavioral sequencing task, mice were imposed to discriminate rewarded corners from never-rewarded corners with acquirement of shuttling behavior between the two distantly positioned rewarded corners to obtain water continuously (**Figure 1B**). No apparent differences in the acquisition of the behavioral sequencing tasks were observed between the control and $NaAsO_2$-exposed groups of both sexes (**Figure 1E**, Figure S4). However, a delay in acquiring the behavioral sequencing tasks was observed in both the control and $NaAsO_2$-exposed females. While the discrimination error rate of both the control and $NaAsO_2$-exposed males was significantly decreased to approximately 10% by session 11 (Figure S4), the discrimination error rate of both groups of females was decreased to approximately 15% by session 21 (**Figure 1E**). It indicates that female mice took longer time to be able to adapt the behavioral sequencing task than that taken by male mice regardless of prenatal exposure to $NaAsO_2$.

In the subsequent serial reversal task, the discrimination error rate for the control and $NaAsO_2$-exposed groups of both female and male mice was elevated in the first session of each reversal phase (Rev 1−11; **Figure 1E**, Figure S4), indicating that each group of both male and female mice properly acquired the behavioral sequence assigned in the previous phase. However, in $NaAsO_2$-exposed female mice, the discrimination error rate was significantly higher than that of the control mice in the first session of reversals 1, 4, 8, and 11, and in the fifth session of reversal 1 (**Figure 1E**). These results suggest that $NaAsO_2$-exposed female mice are impaired in the initial adaptation process of reversal learning. Nevertheless, the increased discrimination error rate in the first session of reversals was significantly reduced in subsequent reversal phase sessions of both groups of female mice (**Figure 1E**), demonstrating a day-to-day improvement in the adaptive behavior in female mice. In male mice, tendency of overall increases in discrimination error rate between the control and and $NaAO_2$-exposed groups was observed. Significant increases were observed in the second session of reversals 5 and 11 (Figure S4), whereas significant decrease in discrimination error rate was found in first session of Rev 6. These results suggest that $NaAsO_2$-exposed male mice showed impairment in adaptation to reversals, but the degree of impairment in males might not be severe compared to that in females.

## Alteration in the Number of Neurons and Glial Cells in the PrL of $NaAsO_2$-Exposed Mice

To determine whether $NaAsO_2$ exposure-related behavioral alterations in mice are associated with changes in brain histology, the number of Cresyl Fast Violet-stained pyramidal neurons, non-pyramidal neurons, and glial cells were measured in three different layers (layer II−III, V, and VI) of the PrL (**Figures 2B,C**). Stereological analysis revealed that the number of pyramidal neurons in layers V and VI but not in layer II−III of the PrL was significantly ($p < 0.05$) increased in the $NaAsO_2$-exposed group as compared to the control group (**Figure 2D**). No significant differences in the number of non-pyramidal neurons and glial cells were observed between the control and *$NaAsO_2$-exposed* groups in any observed layer of the PrL (**Figures 2E,F**).

## Alteration of the Morphology of Neurites in the PrL of $NaAsO_2$-Exposed Mice

We next evaluated the morphology of neurites on Golgi-stained neurons in the PrL. A reduction in the length of neurites on Golgi-stained neurons in the PrL was observed in $NaAsO_2$-exposed mice as compared to neurites in the control group (**Figure 3A**). Space Ball probe analysis indicated that $NaAsO_2$ exposure was associated with a significant ($p < 0.05$) decrease in the length of neurites in Golgi-stained neurons of the PrL as compared to the control group (**Figure 3C**).

## The Density and Morphology of Dendritic Spines of Pyramidal Neurons in the PrL of $NaAsO_2$-Exposed Mice

The density and head diameter of dendritic spines from Golgi-stained pyramidal neurons were measured in three different cortical layers (layer II−III, V, and VI) of the PrL (**Figure 4A**). The total density of dendritic spines in pyramidal neurons was not significantly different between control mice and $NaAsO_2$-exposed mice in any observed layer of the PrL (**Figure 4B**). Spine head diameters were also not significantly different between the